Eur. Phys. J. B **31**, 471–487 (2003)
DOI: 10.1140/epjb/e2003-00057-y

THE EUROPEAN PHYSICAL JOURNAL B

Switching of vortex polarization in 2D easy-plane magnets by magnetic fields

J.P. Zagorodny[1,a], Y. Gaididei[2], F.G. Mertens[1], and A.R. Bishop[3]

[1] Physikalisches Institut, Universität Bayreuth, 95440 Bayreuth, Germany
[2] Institute for Theoretical Physics, 252143 Kiev, Ukraine
[3] Theoretical Division and Center for Nonlinear Studies, Los Alamos National Laboratory, MS B262, Los Alamos, New Mexico 87545, USA

Received 6 June 2002 / Received in final form 4 November 2002
Published online 6 March 2003 –

Abstract. We investigate the dynamics of out-of-plane (OP) vortices, in a 2-dimensional (2D) classical Heisenberg magnet with a weak anisotropy in the coupling of z-components of spins (easy plane anisotropy), on square lattices, under the influence of a rotating in-plane (IP) magnetic field. Switching of the z-component of magnetization of the vortex is studied in computer simulations as a function of the magnetic field's amplitude and frequency. The effects of the size and the anisotropy of the system on the switching process are shown. An approximate dynamical equivalence of the system, in the bulk limit, to another system with both IP and OP *static* fields in the rotating reference frame is demonstrated, and qualitatively the same switching and critical behavior is obtained in computer simulations for both systems. We briefly discuss the interplay between finite size effects (image vortices) and the applied field in the dynamics of OP vortices. In the framework of a *discrete* reduced model of the vortex core we propose a mechanism for switching the vortex polarization, which can account qualitatively for all our results. A coupling between the IP movement (trajectories) of the vortex center and the OP core structure oscillations, due to the discreteness of the underlying lattice, is shown. A connection between this coupling and our reduced model is made clear, through an analogy with a generalized Thiele equation.

PACS. 75.10.Hk Classical spin models – 75.30.Gw Magnetic anisotropy – 75.40.Mg Numerical simulation studies

1 Introduction

The stability and dynamics of spin vortices in ferromagnetic materials have received much attention during the past decades, but nowadays is becoming even more attractive, from both the pure and applied science viewpoints. On the one hand, very recently direct experimental observation of vortices or "curling" states, as stable micromagnetic states of small (submicron) magnetic particles (dots), has been attained thanks to magnetic microscopy techniques with enhanced resolution-magnetic force microscopy (MFM) and Lorentz transmission electron microscopy (LTEM). Notable MFM experiments on circular nanoscale dots of Permalloy ($Ni_{80}Fe_{20}$) [1,2], and Co [2,3] disposed in arrays over nanopatterned films, report images of vortex cores, where the magnetization is found to point out of the plane of the film. LTEM imaging also shows vortices to be favorable configurations in permalloy nanodisks [2,4]. High sensitivity magneto-optical methods have been used [5] to measure the hysteresis loops on Supermalloy ($Ni_{80}Fe_{14}Mo_5$) nanodisks, and the shape of the loops agrees very well with that of calculated loops in micromagnetic simulations of thin disks with vortex states. These experiments have opened the door to directly checking theories of vortices in ferromagnetic materials, making possible an understanding of the interplay between mesoscopic nonlinear collective excitations and geometrical constraints, such as shape, size and boundary conditions at the interfaces (see Ref. [7]). Concerning dynamical properties, it is important to investigate the response of systems with vortex states to applied bias fields, which are control variables in experiments and potential applications. The dynamical effects of nonlinear excitations in finite two-dimensional (2D) and quasi-2D spin systems are especially relevant for read-heads in storage devices, because of the high speeds of transfer reached by today's hard disks. Still, experiments are lacking which can resolve, in space and time simultaneously, and hence numerical simulations of Landau-Lifshitz equations have been the traditional source of data regarding vortex dynamics. Simulation of 2D systems is important because there are many 2D and quasi-2D magnetic materials, in

[a] e-mail: juan.zagorodny@uni-bayreuth.de

the form of mono-layers, layered and intercalated-layered compounds (for a review see Ref. [8,9]), which are known to support nonlinear excitations.

On the other hand, vortices have been shown to be relevant in many fields of theoretical physics, including 2D electron plasmas, 2D superfluid and superconductor systems, and 2D Josephson junction arrays, and it is well established that they drive the topological phase transition of Berezinskii-Kosterlitz-Thouless [10] (BKT). In the continuum approach, exact static solutions for the 2D isotropic Heisenberg model are known, in the form of topological metastable states [11], but as soon as a weak XY-type anisotropy or a magnetic field are included, the topologically non-trivial solutions are not known in a closed analytical form, but only through numerically obtained vortex-like profiles. For the 2D anisotropic easy-plane case, already in the 1980s two kinds of vortices were identified [12]: in-plane (IP) or planar vortices, which are solutions with the magnetization always parallel to the XY-plane, and out-of-plane (OP) vortices, with OP components of the magnetization in the vortex center region or "core", from which only asymptotic behavior was known [12]. Both types of vortices were found to be stable in different regions of the anisotropy parameter (see Hamiltonian (1) below) in numerical simulations, and their asymptotic behavior and deformations due to movement were calculated for each region [13]. In the context of a phenomenology of a dilute gas of vortices, their contributions to low-frequency "central peaks" in dynamical form factors were studied [14,13]. The crossover from IP vortices (for $\lambda < \lambda_c$, see 2) to OP vortices (for $\lambda > \lambda_c$) was also established by analytical arguments [13,15].

Most of the above work was done mainly at zero magnetic fields, which complicated even more the scenario. Although much work has been done on the XY-model ($\lambda = 0$) with static IP magnetic fields [16], little is known about the properties of easy-plane models with magnetic fields for general λ. A field applied in the XY-plane lifts the degeneracy of the ground state and selects a preferential direction. In the presence of a vortex this kind of field can lead to formation of domain walls connecting the vortex core with the boundary of the system.

A magnetic field perpendicular to the easy plane tilts the ferromagnetic IP ground state into the so-called "cone state", in which the z-component of magnetization results from a competition between the OP field and the effective anisotropy field [17]. The IP component of magnetization is still in some arbitrary direction of the plane since the IP isotropy is not broken. The shape of an OP vortex in the presence of such a perpendicular field was calculated [17], and a study of the magnon modes in this system is in progress [18].

The dynamics of OP vortices in easy-plane magnets in an external static field with both IP and OP components has not yet been investigated. In addition, the study of OP vortices in the presence of time-dependent magnetic fields is very limited. Apart from a prior short work in reference [19] where the dynamics of OP vortices in a uniform rotating IP field was investigated for the first time, we are aware of only one work about vortex pairs in a uniform oscillating IP field (Ref. [20]).

In this paper we are concerned with *dynamics* of OP vortices, driven by either an ac rotating IP magnetic field or a static field with both IP and OP components. The switching of the OP components of magnetization of a vortex in a 2D lattice is numerically studied (Sect. 3) for the first case, extending the earlier work of reference [19], and a discrete reduced model of the vortex core (which can account qualitatively for the features of this process) is proposed (Sect. 4). A relation between this system and the one in the second case, which contains only a static field, is explored (Sect. 3) by transforming to a rotating reference frame. In both cases, a coupling between the OP oscillation modes of the vortex structure and the IP movement of the vortex center, while it moves around in the lattice, is seen in the simulations. In the context of our reduced model of the vortex core, a formal connection is found between one of its equations, governing the antisymmetric oscillation modes (Sect. 4.2), and a generalized Thiele equation, that is believed to give a low order approximation to the movement of the vortex center (Appendix B). We have carried out extensive numerical simulations which confirm and extend the results in reference [19]. Our work is theoretical in character, but we briefly discuss in the Conclusions the extent of applicability of our results to real samples of ferromagnets.

2 Hamiltonian, equations of motion and symmetries

In this section we will present a review of our model, which is given by the easy-plane Heisenberg Hamiltonian for classical spins $\boldsymbol{S_n}$ with fixed length S, located on sites $\boldsymbol{n} = (n_x, n_y)$ of a 2D quadratic lattice:

$$\mathcal{H} = -\frac{J}{2} \sum_{\boldsymbol{n},\boldsymbol{n'}} S^x_{\boldsymbol{n}} S^x_{\boldsymbol{n'}} + S^y_{\boldsymbol{n}} S^y_{\boldsymbol{n'}} + \lambda S^z_{\boldsymbol{n}} S^z_{\boldsymbol{n'}}, \qquad (1)$$

where λ is the anisotropy parameter ($0 \leq \lambda < 1$), $J > 0$ is the exchange integral, and the sum over $\boldsymbol{n'} = \boldsymbol{n} + \boldsymbol{a}$ runs over the nearest neighbors of $\boldsymbol{n}$ ($a_x = \pm a, a_y = 0$ or $a_x = 0, a_y = \pm a$, with a the lattice constant). We take S to be dimensionless ($\hbar = 1$) and so J has energy units. In what follows we may also set $J = 1$ and $S = 1$, as well as $a = 1$, when convenient. The limiting cases $\lambda = 0$ (XY-model) and $\lambda = 1$ (isotropic model) have different ground states: the first one has a collinear ground state pointing in some arbitrary direction of the plane, while for the latter one this direction is arbitrary in the whole 3D space.

The interaction with an external magnetic field $\boldsymbol{H_n}(t)$ has the general form

$$V(t) = -\gamma_0 \sum_{\boldsymbol{n}} \boldsymbol{H_n}(t) \cdot \boldsymbol{S_n}, \qquad (2)$$

where the gyromagnetic factor $\gamma_0 \equiv 2\mu_0\mu_{\mathrm{B}}$, with μ_0 the vacuum permitivity and μ_{B} the Bohr magneton (in MKS,

when $\hbar \neq 1$, $\gamma_0 \equiv 2\mu_0\mu_B/\hbar = 0.221 \frac{\mathrm{MHz}}{\mathrm{A/m}}$), will be absorbed from now on in a field $\boldsymbol{h}_{\boldsymbol{n}}(t) \equiv \gamma_0 \boldsymbol{H}_{\boldsymbol{n}}(t)$ having the same units as J.

The spin dynamics is described by the Landau-Lifshitz (LL) equations, which in normalized form can be written as

$$\frac{\mathrm{d}\boldsymbol{S}_{\boldsymbol{n}}}{\mathrm{d}t} = -\boldsymbol{S}_{\boldsymbol{n}} \times \frac{\partial\,[H + V(t)]}{\partial \boldsymbol{S}_{\boldsymbol{n}}} + \varepsilon\, \boldsymbol{S}_{\boldsymbol{n}} \times \left(\boldsymbol{S}_{\boldsymbol{n}} \times \frac{\partial H}{\partial \boldsymbol{S}_{\boldsymbol{n}}} \right). \tag{3}$$

With $1 \leq n_x, n_y \leq N$, these are $3N^2$ equations which preserve the lengths of the spins $|\boldsymbol{S}_{\boldsymbol{n}}| = S$. We have added to the LL equations a phenomenological damping term *à la* Landau [21], with a small dimensionless parameter ε. We did not include in this term some contribution coming from the interaction with the external field, having in mind a damping which arises from the exchange interaction (see remarks in Appendix A). We will consider here spin dynamics under the influence of a spatially uniform in-plane (IP) rotating field

$$\boldsymbol{h}(t) = h\,(\cos(\omega t + \alpha_0),\ \sin(\omega t + \alpha_0),\ 0) \tag{4}$$

with amplitude h, frequency ω and initial phase α_0, which is switched on at $t = 0$. We may put in general $\alpha_0 = 0$, but, as we will see, the initial orientation of the field has some visible consequences on the trajectories of vortices. We are interested in weak and slowly varying fields $h, \omega \ll J$, so as not to perturb the states at zero field significantly, and also small damping $\varepsilon \ll 1$.

For typical quasi-2D ferromagnetic materials with easy-plane symmetry (for instance K_2CuF_4, a layered magnet with a ratio of interplane-to-intraplane exchange constants $J'/J \approx 10^{-4}$, see Ref. [6]), at low temperature ($T_c \approx 6.25\,\mathrm{K}$), with an exchange interaction $J \approx 10\,\mathrm{K}$ and anisotropies ranging from 1 to 10% ($\lambda \approx 0.99$ to 0.9 resp.), the anisotropy field, given by $\gamma_0\, H_a = 4J(1-\lambda)$, is in the range $H_a \approx 3$ to 30 kOe [6,18]. Corresponding resonances are in the range $\omega_a \equiv \gamma_0 H_a \approx 50$ to 500 GHz, respectively. The field intensities we used in our simulations of Section 3 are in the order $h \approx 10^{-3}J$, which for the above value of J represent a field intensity $H \approx 74.4\,\mathrm{Oe} \ll H_a$. For an estimation of the frequencies, we have to restore the value of $\hbar$. Our dimensionless time variable has then a scaling factor $\omega_0 = J/\hbar \approx 1.3\,\mathrm{THz}$, so the typical frequencies in our simulations are in the range $\omega \approx 10^{-3}\omega_0$ to $10^{-2}\omega_0 \approx 1\,\mathrm{GHz}$ to $10\,\mathrm{GHz} \ll \omega_a$, in most of our simulations ($\lambda = 0.9$).

In considering spins of fixed length, it is convenient to have the above expressions in terms of polar angles: $\boldsymbol{S}_{\boldsymbol{n}} = S\{\sin\Theta_{\boldsymbol{n}} \cos\Phi_{\boldsymbol{n}}, \sin\Theta_{\boldsymbol{n}} \sin\Phi_{\boldsymbol{n}}, \cos\Theta_{\boldsymbol{n}}\}$. The Hamiltonian now reads

$$H = -\frac{JS^2}{2} \sum_{\boldsymbol{n},\boldsymbol{n}'} \{\, P_{\boldsymbol{n}}\, P_{\boldsymbol{n}'}\, \cos(\Phi_{\boldsymbol{n}} - \Phi_{\boldsymbol{n}'}) + \lambda\, M_{\boldsymbol{n}}\, M_{\boldsymbol{n}'}\}, \tag{5}$$

where $M_{\boldsymbol{n}} = \cos\Theta_{\boldsymbol{n}}$ is the on-site z-component of the magnetization, canonically conjugated to $\Phi_{\boldsymbol{n}}$, and we defined $P_{\boldsymbol{n}} \equiv \sqrt{S^2 - M_{\boldsymbol{n}}^2} = \sin\Theta_{\boldsymbol{n}}$. The interaction with the field takes the form

$$V(t) = -hS \sum_{\boldsymbol{n}} P_{\boldsymbol{n}}\, \cos(\Phi_{\boldsymbol{n}} - \omega t - \alpha_0), \tag{6}$$

and the $3N^2$ "Cartesian" LL equations reduce to the $2N^2$ "polar" equations

$$\begin{aligned} \dot{\Phi}_{\boldsymbol{n}} &= \frac{\partial\,[H + V(t)]}{\partial M_{\boldsymbol{n}}} - \frac{\varepsilon}{1 - M_{\boldsymbol{n}}^2} \frac{\partial H}{\partial \Phi_{\boldsymbol{n}}} \\ \dot{M}_{\boldsymbol{n}} &= -\frac{\partial\,[H + V(t)]}{\partial \Phi_{\boldsymbol{n}}} - \varepsilon\,(1 - M_{\boldsymbol{n}}^2)\, \frac{\partial H}{\partial M_{\boldsymbol{n}}}. \end{aligned} \tag{7}$$

This latter form will be useful for analytical considerations. Notice that at zero damping these are the Hamilton equations for the system. It is worth noticing also that equations (5–7) (and also Eqs. (A.3) of Appendix A, in angular variables), are invariant under the transformation

$$M_{\boldsymbol{n}} \to -M_{\boldsymbol{n}},\ \ \Phi_{\boldsymbol{n}} \to -\Phi_{\boldsymbol{n}},\ \ \omega \to -\omega,\ \ \alpha_0 \to -\alpha_0, \tag{8}$$

which has consequences for the dynamics of vortices in the presence of our ac magnetic field (see next section). An IP *static* field would then be represented by a vanishing frequency $\omega = 0$ in the formulas above, and the symmetry (8) would be reached with the sole change $\alpha_0 \to -\alpha_0$, *i.e.*, $h_y \to -h_y$. A perpendicular *static* field $\boldsymbol{h} = h_z\hat{\boldsymbol{z}}$ would add an interaction term

$$W = -h_z \sum_{\boldsymbol{n}} S_{\boldsymbol{n}}^z = -h_z S \sum_{\boldsymbol{n}} M_{\boldsymbol{n}} \tag{9}$$

and the symmetry (8) would then require $h_z \to -h_z$.

2.1 Static configurations and vortices

Vortices in this system are known to be stable excitations characterized by two non-null topological charges. Topological properties must be understood in terms of continuum descriptions. Although we will work with our model directly in discrete form, we need to present at least some definition of vortex solutions in a continuum description. Further details can be found in references [9,23–25]. By expanding $\boldsymbol{S}_{\boldsymbol{n}+\boldsymbol{a}}$ up to 2nd order around $\boldsymbol{S}_{\boldsymbol{n}}$, the Hamiltonian (1) results in

$$H = -\frac{J}{2} \int \mathrm{d}^2x\, \left\{ \boldsymbol{S} \cdot \Delta\boldsymbol{S} - \delta S_z\, \Delta S_z - \frac{2\delta}{a^2}\, S_z^2 \right\},$$

where $\delta = 1 - \lambda$ and a constant $H_0 = -2JS^2N^2$ was dropped. This can also be expressed in canonical variables $M(x,y,t)$ and $\Phi(x,y,t)$. Adding an interaction with a static field with both IP and perpendicular components

$$V = -\frac{S}{a^2} \int \mathrm{d}^2x \left\{ h\sqrt{1 - M^2}\, \cos(\Phi - \alpha_0) + h_z\, M \right\}$$

will give a homogeneous ground state with $\Phi = \alpha_0$ or $\alpha_0 + \pi$, and M resulting from the quartic equation

$$(1 - M^2)(h_z - 2JS\delta M)^2 - h^2 M^2 = 0, \tag{10}$$

which shows the competition between the fields and the anisotropy. In particular, the case of a pure IP field finds a minimum of the energy in the trivial planar solution ($M = 0$ or $\Theta = \pi/2$). The case of a pure out-of-plane (OP) field gives the cone state [17]: $M = \cos\Theta = h_z/(2\delta JS)$, where Φ is not constrained. Finally for the isotropic case ($\delta = 0$) we have a tilted collinear state with $M = \pm h_z/\sqrt{h^2 + h_z^2}$, again with $\Phi = \alpha_0$ or $\alpha_0 + \pi$.

The simplest static (and the only exactly known) vortex solution at zero field is an IP vortex

$$M(\boldsymbol{r}) = 0, \quad \Phi(\boldsymbol{r}) = Q \arctan\left(\frac{y-Y}{x-X}\right) + \varphi_0 \qquad (11)$$

which is singular at $(X, Y) \equiv \boldsymbol{X}$, the coordinates of the vortex center. The constant φ_0 will only set the relative orientation of the vortex with respect to an IP field which breaks the IP isotropy [16], otherwise it is irrelevant: considering how Φ couples to a magnetic field in (6), we see that φ_0 can be absorbed into α_0.

The vorticity of an arbitrary configuration is defined by the circulation integral

$$Q = \frac{1}{2\pi} \oint \boldsymbol{\nabla}\Phi(\boldsymbol{r}, t) \cdot \mathrm{d}\boldsymbol{r}$$

and will be a non-null integer only if the contour of integration encloses the center of a vortex. The total Q is a conserved charge during the time evolution of the configurations in the present model. A discrete version of the circulation condition over the azimuthal angles $\Phi_{\boldsymbol{n}}$ in the presence of a vortex can be formulated [10] as

$$\sum_{\gamma(\boldsymbol{n})} \Delta\Phi(\boldsymbol{n}, t) = 2\pi Q \qquad (12)$$

where Δ is the first difference operator along a closed path $\gamma(\boldsymbol{n})$ on the lattice. This gives a practical criterion to find in which plaquette (unit cell) of the lattice the center of a vortex lies. A further refinement for finding a better estimate for the position of the vortex center within a plaquette, in the simulations, is described in reference [25].

The existence of two kinds of vortices (IP vortices like (11), stable for $\lambda < \lambda_c$ and OP vortices with $M_{\boldsymbol{n}} \neq 0$, stable for $\lambda_c < \lambda < 1$, where $\lambda_c \simeq 0.72$ for a square lattice) is already well established in numerical simulations [13]. In reference [15] the so-called "out-of-plane instability" around a lattice-dependent critical value λ_c was studied analytically within the context of a reduced model of the core of a vortex. The OP structure of static vortices shows a characteristic asymptotic behavior [13] in polar coordinates of the plane $(x, y) = (r\cos\varphi, r\sin\varphi)$:

$$M(r) = \begin{cases} \pm\left(1 - \frac{b^2 r^2}{2r_v^2}\right), & \text{for } r \to 0, \\ \pm c\sqrt{\frac{r_v}{r}} \exp\left[-r/r_v\right], & \text{for } r \to \infty, \end{cases}$$

where

$$r_v = a\sqrt{\lambda/(1-\lambda)}/2 \qquad (13)$$

is interpreted as the radius of the vortex core, or characteristic length of the OP structure, and b and c are constants to be adjusted by matching the two expressions at $r = r_v$. This exponential behavior is a particular feature of magnetic vortices, in contrast to vortices in other fields, like superfluids, etc.

In addition, magnetic vortices carry a second topological charge: for 2D models where OP structures can be stable (*e.g.*, when $\lambda > \lambda_c$) we must consider a second topological invariant, sometimes called the Pontryagin index:

$$\Gamma = \frac{1}{4\pi}\int_\sigma g\,\mathrm{d}x\mathrm{d}y = \frac{-1}{4\pi}\int_\sigma \sin\Theta\,\mathrm{d}\Theta\mathrm{d}\Phi$$
$$g = (\partial_x \boldsymbol{S} \times \partial_y \boldsymbol{S}) \cdot \boldsymbol{S} = \boldsymbol{\nabla} M(\boldsymbol{r}, t) \times \boldsymbol{\nabla}\Phi(\boldsymbol{r}, t) \cdot \hat{\boldsymbol{z}},$$

where the area σ encloses the excitation, but is arbitrarily shaped. We term g "gyro-coupling" density, following Thiele [26]. OP vortices are gyrotropic excitations in the sense that their dynamics in the continuum limit conserves the gyrovector $\boldsymbol{G} = G\hat{\boldsymbol{z}}$, where $G = 4\pi\Gamma$. Collective variable theories for the movement of the centers of both OP (gyrotropic) and IP (non-gyrotropic) vortices, always in the continuum limit, have been developed [25]. The gyrovector of a vortex with the IP structure (11) but for general $M(\boldsymbol{r})$ is easily calculated [27] at zero field, by giving proper physical boundary conditions $M(\boldsymbol{r} = \boldsymbol{X}) = \pm 1, M(r \to \infty) = 0$, resulting in

$$\boldsymbol{G} = -2\pi Q\,\hat{\boldsymbol{z}}[M(\boldsymbol{r} = \boldsymbol{X}) - M(r \to \infty)] = -2\pi Q\, p\,\hat{\boldsymbol{z}}, \qquad (14)$$

where $p = M(\boldsymbol{r} = \boldsymbol{X}) = \pm 1$ is the magnetization in the center of the vortex, or the polarization. It is easily seen that a magnetic field will modify this result. For instance, a weak perpendicular field pointing in the $+\hat{\boldsymbol{z}}$ direction, will tilt the spins sited far from the vortex core, where they lie in the plane, towards above the plane. Depending on whether the vortex has $\boldsymbol{G}$ parallel or antiparallel to the field ("light" or "heavy" vortex, respectively [17,18], see Sect. 3.4), this field will enhance the region of the core, where the spins are more perpendicular to the plane, or will reduce it, respectively.

Since both Q and $\Gamma = -\frac{1}{2}Qp$ are invariants, it follows that p is also conserved during the dynamics of a single vortex in the continuum limit. This is not a constraint, however, for a discrete system.

In a discrete model, G can be rewritten in first finite difference approximation [28] as

$$G = \frac{1}{4\pi}\sum_{\boldsymbol{n}} (\boldsymbol{S}_{\boldsymbol{n}+\boldsymbol{a}} - \boldsymbol{S}_{\boldsymbol{n}-\boldsymbol{a}}) \times (\boldsymbol{S}_{\boldsymbol{n}+\boldsymbol{b}} - \boldsymbol{S}_{\boldsymbol{n}-\boldsymbol{b}}) \cdot \boldsymbol{S}_{\boldsymbol{n}}, \qquad (15)$$

where $\boldsymbol{a} = a\hat{\boldsymbol{x}}, \boldsymbol{b} = a\hat{\boldsymbol{y}}$ are basis vectors of the lattice. This quantity is generally not conserved during the dynamics of the discrete system, equations (3), which allows processes such as the switching of polarization shown in the next sections.

On the other hand, stability conditions, which should be fulfilled by any static configuration, are obtained from

the variation of the Hamiltonian (5), *i.e.*

$$\frac{\partial H}{\partial \Phi_{\boldsymbol{n}}} = 0 = P_{\boldsymbol{n}} \sum_{\boldsymbol{a}} P_{\boldsymbol{n}+\boldsymbol{a}} \sin(\Phi_{\boldsymbol{n}} - \Phi_{\boldsymbol{n}+\boldsymbol{a}}) \tag{16}$$

$$\frac{\partial H}{\partial M_{\boldsymbol{n}}} = 0 = \frac{M_{\boldsymbol{n}}}{P_{\boldsymbol{n}}} \sum_{\boldsymbol{a}} P_{\boldsymbol{n}+\boldsymbol{a}} \cos(\Phi_{\boldsymbol{n}} - \Phi_{\boldsymbol{n}+\boldsymbol{a}}) - \lambda \sum_{\boldsymbol{a}} M_{\boldsymbol{n}+\boldsymbol{a}}, \tag{17}$$

where we have not included a possible contribution from static magnetic fields, which will have in general the effect of deforming any configuration, including vortices. It is important to stress that *a strong enough magnetic field can even destroy vorticity in the finite system.*

For an IP vortex the condition (16) becomes

$$\sum_{\boldsymbol{a}} \sin(\Phi_{\boldsymbol{n}} - \Phi_{\boldsymbol{n}+\boldsymbol{a}}) = 0 \tag{18}$$

while for OP vortices this is only approximate, for the region far from the core, where $P_{\boldsymbol{n}}$ approaches unity.

In a previous work [19], the first results were presented concerning the dynamics of an OP vortex in the presence of a weak magnetic field of the form (4). The analytic work was restricted to small amplitude fields, which made it possible to treat the field as a small perturbation. In the next sections we will extend these calculations in the framework of a reduced discrete model, and numerically explore more details of the system, concentrating on the "flipping" times (see Sect. 3) and searching for the effects of variations in the size and anisotropy of the system.

Due to the approximate azimuthal symmetry of the static vortex IP structure it is convenient to work on a lattice with a circular boundary, so that we can set the conditions at the boundary more easily *via* the image method, with only one image per vortex, in analogy with a 2D electrostatic problem. The static interaction between two such IP vortices, at zero field, has the well-known [10] logarithmic form

$$E = -2\pi J S^2 Q_1 Q_2 \ln|\boldsymbol{X}_1 - \boldsymbol{X}_2|, \tag{19}$$

where $\boldsymbol{X}_i = (X_i, Y_i)$ are the coordinates of the ith vortex center ($i = 1, 2$) in the plane. The deviation from this law for OP vortices in the easy-plane case ($\lambda_c < \lambda < 1$) is negligible at distances much larger than the typical size of the cores r_v, as given by (13) such that the OP structures do not overlap. In the presence of an IP magnetic field the mutual interaction between IP vortices was estimated for the XY model ($\lambda = 0$): it becomes linear for large distances due to the field, and no BKT phase transition is then expected since this field removes the continuous degeneracy of the ground state (see for instance Ref. [16]).

Vortices with $|Q| > 1$ are known to decay rapidly to $|Q| = 1$ vortices, radiating spin waves, so we can consider here only the $|Q| = 1$ case. In the case of a circular system with radius R_0 and free boundary conditions, the azimuthal angles $\Phi_{\boldsymbol{n}}$ (the IP structure) for both IP and OP static vortices are given approximately by the superposition

$$\Phi^0_{\boldsymbol{n}} = \arctan\left(\frac{n_y - Y}{n_x - X}\right) - \arctan\left(\frac{n_y - \bar{Y}}{n_x - \bar{X}}\right), \tag{20}$$

where $\bar{X} = XR_0^2/R^2$, $\bar{Y} = YR_0^2/R^2$ ($R^2 = X^2 + Y^2$) are the coordinates of the image vortex. In the case of fixed boundary conditions the sign in front of the second term in equation (20) is reversed. In the discrete case, equation (20) is only an approximate solution of the extreme condition (18) for the in-plane static configuration, suitable for setting initial conditions for simulations. In contrast, the condition (12) accompanies even the mobile vortices.

2.2 Symmetries of the model: vortices and magnetic fields

We return now to the symmetry (8). We use the label "up" for the direction $+\hat{\boldsymbol{z}}$. It is easy to see that the two first changes in (8) transform a vortex configuration pointing up ($Q = 1, p = 1$) into an antivortex pointing down ($Q = -1, p = -1$). Accordingly, the dynamics of an up-vortex in a field anti-clockwise "up" ($\boldsymbol{\omega} = \omega\hat{\boldsymbol{z}}$, with $\omega > 0$), initially pointing towards, say, the positive $\hat{\boldsymbol{y}}$ direction ($\alpha_0 = \pi/2$) is indistinguishable from the dynamics of a down-antivortex in a clockwise "down" field $\omega < 0$, initially pointing in $-\hat{\boldsymbol{y}}$ direction ($\alpha_0 = -\pi/2$). In this way, out of the 16 combinations of signs of (Q, p, α_0, ω) only 8 have a different dynamics, as can be seen from Table 1. This is quite natural, considering that the infinite system is invariant upon reversal of the z-axis , as is the case with the finite system, where the border is circular so as not to select preferential directions. This is confirmed in our numerical simulations in circular systems, whose details are explained in the next sections.

Out of the 8 independent combinations, we have 2 scenarios: the 4 systems for which the "angular velocity" $\boldsymbol{\omega} = \omega\,\hat{\boldsymbol{z}}$ of the field is antiparallel to the initial vortex polarization ($p\,\omega < 0$) are seen to produce during the dynamics (for a strong enough field, to be quantified later) a switch in the sign of the whole OP vortex structure (referred to as "flip" or "switching"), in particular $p \to -p$, while those 4 systems whose $\boldsymbol{\omega}$ is parallel to the initial polarization ($p\,\omega > 0$) do not show a flip (see next sections for details).

The same picture is recovered for an equivalent system with one vortex and a static field with both IP and OP components, in the reference frame which rotates with frequency ω: one field component in an arbitrary direction in the plane, say $\hat{\boldsymbol{y}}$ (if we put $\alpha_0 = \pm\pi/2$ as in Tab. 1), with strength $h_y = \pm h$, and the other component in the z-direction with strength $h_z = \pm\omega$. The equivalence, strict only in the bulk, proceeds as follows. In the frame of reference which rotates together with the magnetic field,

Table 1. Combinations of charges of a single vortex and signs of parameters of magnetic fields. (α_0, ω) refer to the rotating field (4), while (h_y, h_z) refer to a static field with both IP and OP components. The numbers at the left and right of the table show systems with indistinguishable dynamics.

	Q	p	α_0 or h_y	ω or h_z	$Q\,\alpha_0$	$p\,\omega$	
1	+1	+1	+1	+1	+1	+1	16
2	+1	+1	+1	−1	+1	−1	15
3	+1	+1	−1	+1	−1	+1	14
4	+1	+1	−1	−1	−1	−1	13
5	+1	−1	+1	+1	+1	−1	12
6	+1	−1	+1	−1	+1	+1	11
7	+1	−1	−1	+1	−1	−1	10
8	+1	−1	−1	−1	−1	+1	9
9	−1	+1	+1	+1	−1	+1	8
10	−1	+1	+1	−1	−1	−1	7
11	−1	+1	−1	+1	+1	+1	6
12	−1	+1	−1	−1	+1	−1	5
13	−1	−1	+1	+1	−1	−1	4
14	−1	−1	+1	−1	−1	+1	3
15	−1	−1	−1	+1	+1	−1	2
16	−1	−1	−1	−1	+1	+1	1

$\Phi_{\boldsymbol{n}} - \omega t = \Psi_{\boldsymbol{n}}$, the LL equations (7) take the form

$$\dot{\Psi}_{\boldsymbol{n}} = \frac{\partial}{\partial M_{\boldsymbol{n}}}(H+V) - \frac{\varepsilon}{1-M_{\boldsymbol{n}}^2}\frac{\partial H}{\partial \Psi_{\boldsymbol{n}}} + \omega$$
$$\dot{M}_{\boldsymbol{n}} = -\frac{\partial}{\partial \Psi_{\boldsymbol{n}}}(H+V) - \varepsilon\,(1-M_{\boldsymbol{n}}^2)\,\frac{\partial H}{\partial M_{\boldsymbol{n}}}. \quad (21)$$

Hence, in this frame the dynamics is equivalent to that of a system with a static field with both an IP component $\boldsymbol{h}_1 = h(\cos\alpha_0, \sin\alpha_0, 0)$, which produces the interaction

$$V = -\sum_{\boldsymbol{n}} \boldsymbol{S}_{\boldsymbol{n}} \cdot \boldsymbol{h}_1 = -\,h \sum_{\boldsymbol{n}} P_{\boldsymbol{n}}\,\cos(\Psi_{\boldsymbol{n}} - \alpha_0), \quad (22)$$

and an OP component $\boldsymbol{h}_2 = (0, 0, -\omega)$ aligned along the angular velocity $\boldsymbol{\omega}$, which produces the interaction

$$W = -\sum_{\boldsymbol{n}} \boldsymbol{S}_{\boldsymbol{n}} \cdot \boldsymbol{h}_2 = \omega \sum_{\boldsymbol{n}} M_{\boldsymbol{n}}. \quad (23)$$

In this case vortices for which $p\,h_z < 0$ are called "heavy" vortices [18] and are seen to flip to "light" vortices during the dynamics, while "light" vortices ($p\,h_z > 0$) remain stable.

For our investigations below, it is sufficient to carry out simulations with vortices ($Q = 1$), up and down ($p = \pm 1$) with respect to $\hat{\boldsymbol{z}}$.

3 Computer simulation results

We have carried out extensive computer simulations with OP vortices in the presence of a rotating field. We have numerically integrated the full Landau-Lifshitz equations (3), for square lattices of several sizes (with $N^2 \equiv L^2 = 48^2, 72^2, 96^2$, and 120^2 spins), taking care of distinguishing those cases when the vortex dynamics has a stronger influence from the external magnetic field from those cases in which the influence from the image-vortex field is stronger. In each lattice the system is defined by a circular border with diameter $L = 2R_0$, in order to more easily set free boundary conditions: for a vortex ($Q = 1$) with polarization up ($p = 1$) at the position $\boldsymbol{X} = (X, Y)$, only one image anti-vortex ($Q = -1$) with polarization up at the position $\bar{\boldsymbol{X}} = (\bar{X}, \bar{Y})$ is needed.

For most of the simulations, unless otherwise stated, the values of anisotropy ($\lambda = 0.9$) and damping ($\varepsilon = 0.002$) were set as in reference [19]. At this λ, the typical radius, or characteristic length, of the OP structure of the vortex, given by the continuum limit (13) is around 1.5 lattice constants, although, as can be seen in Figure 8a, non-negligible z-components of the spins extend in fact well up to 2.5 lattice sites in each direction.

We have studied mainly the system of diameter $L = 72$ with free boundary conditions, for which we present a detailed phase diagram of flip events in the space of the parameters (ω, h) of the magnetic field. We used relatively weak amplitude fields so as neither to change the ground state significantly, nor to destroy the vortex. The integration time for this phase diagram was set to a maximum of 25,000 time units, in a 4th order Runge-Kutta integration method with time step 0.01, although we performed some special simulations to much longer times. Some further details of the numerical procedures employed, such as the generation of the initial vortex configuration and the way to calculate the vortex core position at each time, are described in the Appendix of reference [25].

3.1 Summary of prior results

It was shown in reference [19] that due to the action of an IP rotating magnetic field the z-component of all spins in the core of an OP vortex, and therefore the vortex polarization $p \equiv M_z(\boldsymbol{n} = \boldsymbol{R})$, can abruptly change in sign, so that the whole vortex OP structure is reversed from one side of the lattice plane to the other (we refer to this event as a "flip" or "switch", see Fig. 1) provided that the amplitude of the field is higher than a certain critical value h_{cr} which depends on the frequency and the initial vortex polarization, but not on the vorticity. The authors of that work used a square lattice with circular boundary of diameter $L = 48$, and presented for this system a curve of the critical amplitude as a function of ω. Starting with a vortex with polarization $p = 1$ it was found that the threshold value $h_{cr}(\omega)$ for a clockwise rotating field ($\omega < 0$), was much smaller than that for counter-clockwise ($\omega > 0$) field. In the latter case the final structure of the vortex was often destroyed by spin waves. Exactly the inverse situation occurred when they used a vortex with $p = -1$ as initial condition: this time the switch to $p = 1$ was favored for a counter-clockwise rotating field.

The switch of the magnetization was thus found to be a unidirectional event: a vortex state with a determined polarization and not the opposite one is favored by the rotating field, so that only when the product $\omega\,p < 0$ does the final state of the vortex have a well defined structure.

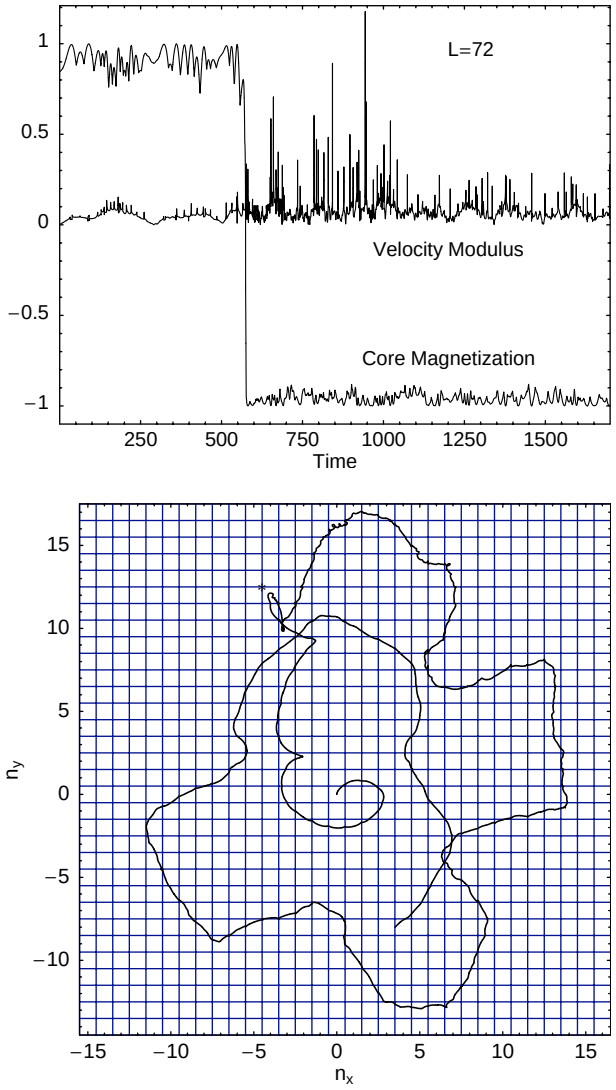

Fig. 1. Above: Typical time evolution of the core magnetization (average of $M_{\boldsymbol{n}}$ over the 4 inner spins) of a vortex ($q = 1$), initially pointing up ($p = 1$), showing a flip at $t \sim 574$ in a weak rotating field $\omega = -0.05$, $h = 0.0024$. The time evolution of the velocity modulus of its center is also shown. Data from numerical simulations of the full LL equations (3), on a square lattice with circular boundary of diameter $L = 72$. Below: Typical vortex trajectory, corresponding to the time evolution shown above, until a longer time $t = 2,600$. Starting from the center $(0, 0)$ of the lattice, it turns clockwise very irregularly. The flip occurs in the part of the trajectory signaled by an asterisk. The intersections of grid lines are the lattice sites.

The basic reason for the switching was argued to be easily understood by using the frame of reference which rotates together with the magnetic field: $\Phi_{\boldsymbol{n}} - \omega t = \Psi_{\boldsymbol{n}}$. As explained in Section 2.2 the vortex feels effectively a static field with both IP and OP components. The perpendicular component clearly breaks the up-down symmetry and thus the vortex states with different polarizations are not equivalent, the switching process becoming energetically favored. It was noticed, however, that this argument does not explain why the threshold amplitude for the switching is a non-monotonic function of the frequency ω. This explanation seems a difficult task, considering the number of parameters which are potentially playing a role. Our reduced model of the next sections will not account for flip times, which we believe to be determined by the complexity of the full many-body system, but rather for qualitative features of the process.

3.2 Results of new sets of simulations

The results of reference [19] are substantially confirmed in the simulations of the present work. We first note, however, that some main conclusions in that paper were drawn from simulations at $|\omega| = 0.1$, which was found to be close to the frequency of the lowest radially symmetric eigenmode in the presence of a vortex [15,31,32]. We have realized meanwhile that $|\omega| = 0.1$ is already a rather high frequency, as can be seen from considerations of the ground state, analogous to those which led to the equation (10) in Section 2.1, for $J = S = 1$ and $\lambda = 0.9$. For the same reason, when we present the size-dependence of the flipping time, and a phase diagram of flip events in the space of field parameters (ω, h), we do so for values $|\omega| < 0.1$.

Secondly we note that the argument in the Section 3.1 can also not be applied to the limiting case $\omega \to 0$, *i.e.*, of an OP vortex driven by a constant IP field. The transformation to the "rotating" frame of reference makes no sense here. It is clear that in this case the perturbation does not break the up-down symmetry. We mention, however, that in a set of our simulations with $\omega = 0$ (static IP field) we also find switching behavior. In this case there can be back switches, as expected from the symmetry, provided that the system is large enough to observe these successive flips before the vortex leaves the lattice through the boundary. Concerning this case, we believe that the magnon (up-down symmetric) perturbation produced by the static field interacting with the moving vortex can be responsible for a flip to occur, as is the case when the perturbation is thermal noise [30]. We will not study the case of $\omega = 0$ any further here.

In Figures 1–2 we show some typical results of the simulations for a system of diameter $L = 72$ in a rotating field ($\omega = -0.05, h = 0.0024$). In Figure 1 above, we plot the core magnetization, *i.e.*, the average of $M_{\boldsymbol{n}}$ over the 4 inner spins of the vortex.

The velocity modulus is also plotted, in order to observe (a) the correlations between these two signals and (b) the increasing velocity fluctuations immediately following the flip. The latter is a clear finite size effect: the flip process produces a circular spin wave propagating outwards, which is reflected at the boundary in a non-symmetric way because the vortex is not at the center of the lattice at the moment of flipping. After some time these waves are damped out because of the damping term we added in the equation (3). The fluctuations in the core magnetization are in any case smaller after the flip than before, showing the larger stability of the vortex whose gyrovector is parallel to the angular velocity $\boldsymbol{\omega}$ of the field.

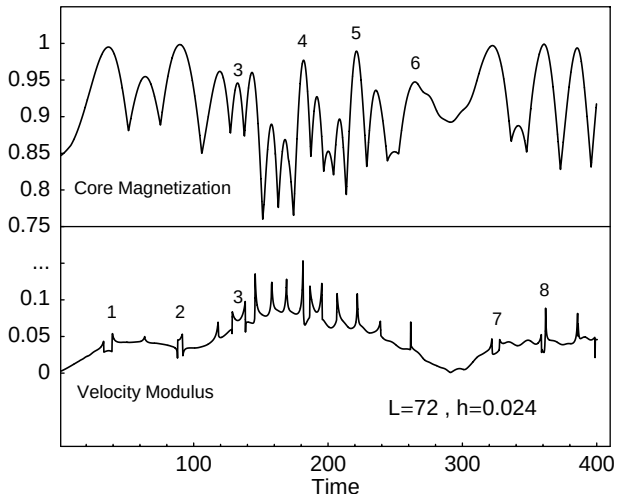

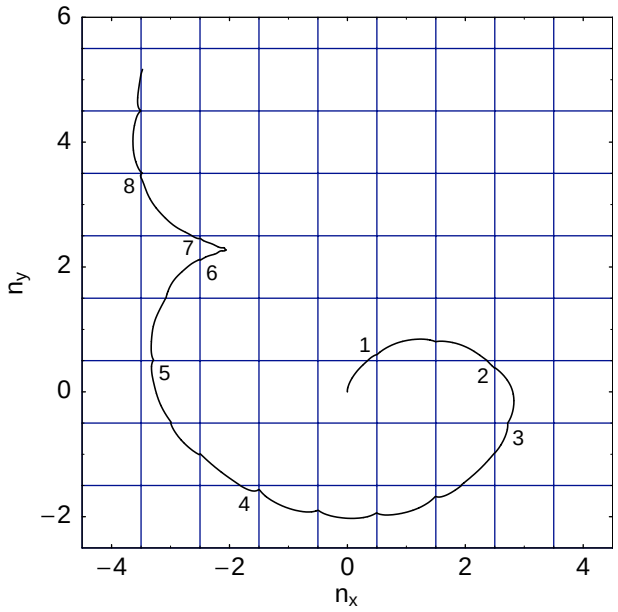

Fig. 2. Above: Zoom-in of a small section of Figure 1 (above), showing correlation between core magnetization and velocity signals, *i.e.* between out-of-plane oscillations and in-plane movement. Below: Initial section of trajectory from Figure 1 (below) enhanced, corresponding to the time evolution shown in Figure 2 above. Starting from the center and clockwise, some events of crossing the saddles of the lattice potential are shown, to be identified with corresponding events (minima and maxima) in Figure 2 above.

We also plot sections of the trajectory, traced by the successive positions of the vortex center. Since the main goal of this paper is to study the vortex flip process, a complete analysis of trajectories will be deferred to a forthcoming work. Here we only show a small trajectory section as reference, to illustrate how the vortex movement over the Peierls-Nabarro periodic potential of the lattice has the effect of coupling the in-plane movement with the oscillations in z-direction of the vortex core magnetization (see Sect. 3.3).

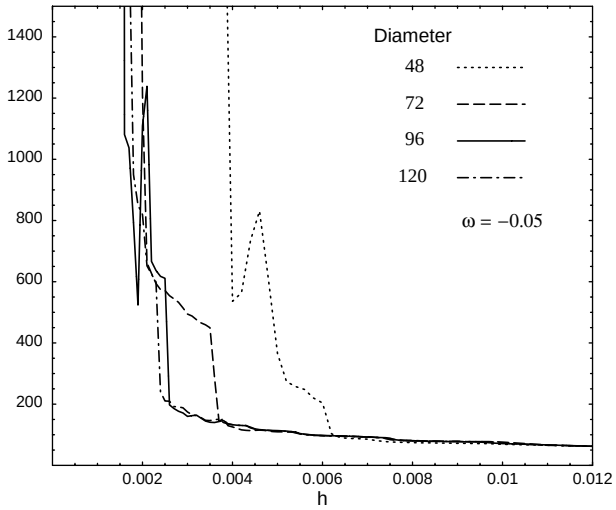

Fig. 3. Non-monotonous size effects: flip time *vs.* (in-plane, rotating) field amplitude h, for a field frequency $\omega = -0.05$, in circular systems of several diameters, obtained from the numerical integration of the full Landau-Lifshitz equations, with damping $\varepsilon = 0.002$ and anisotropy $\lambda = 0.9$. For $h \gtrsim 0.0065$ the differences are negligible for the sizes considered.

We have noted also that when the anisotropy approaches the instability region close to λ_c we can have reverse flips (Fig. 6), but the prior result about uni-directionality of flips is strictly correct at the value $\lambda = 0.9$, at which most of the simulations in reference [19] and ours were performed.

Among the questions opened by reference [19] is the relative influence of the boundary (size effects) and the magnetic field on the switching of vortex polarization. We have extended in this work the numerical simulations to include the sizes mentioned at the beginning of this section. The size effects can be seen in Figures 3–4. In Figure 3 the flip time *vs.* field amplitude h, for the frequency $\omega = -0.05$, is shown for several sizes. We can see from this figure, first that the flip times increase mainly with decreasing amplitudes (up to some non-monotonic jumps), which gives one confidence to speak reasonably about a critical amplitude, or a threshold field, for the flipping process to occur. It must be emphasized that all the simulations can be carried out in a finite observation time, so the critical curve (Fig. 5) is determined as that curve which separates fast events of flips from very late or impossible ones. Except for the critical region at very low amplitudes, the flip process is in general a relatively rapid event, of some hundreds of time units, in all the simulations. Very long simulations ($t \gtrsim 25,000$) will start to find accuracy problems. This number is about the limit when the energy of the system at zero damping and zero field stops being constant due to the presence of accumulative numerical errors. In the prior work [19], the simulations were stopped immediately after a flip was detected, with a maximum time of 12,000 time units. We have continued all our simulations after the flips, to see in more detail the final states, and we have set a maximum time of 25,000 time units.

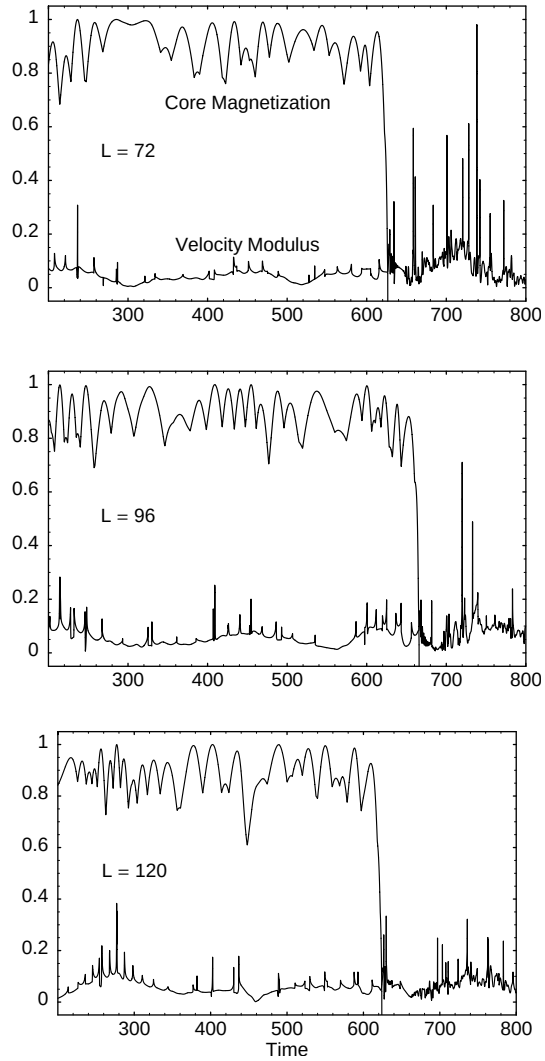

Fig. 4. Time evolution of the core magnetization and the velocity modulus, as in Figure 1 (above), of a vortex in a magnetic field ($\omega = -0.05, h = 0.0022$) for 3 different sizes.

Figure 3 also gives insight into the relative effects of the size of the system on the flip time. It tells us that the prior results in reference [19] were obtained for a rather small lattice. We can see that the present system with diameter $L = 72$ spins is much closer to what we can expect as bulk behavior, minimizing thus the size effects. We can expect relatively small size effects whenever we consider amplitudes $h \gtrsim 0.004$ (for frequency $\omega = -0.05$), over a wide range of sizes from $L = 72$ up to the bulk, as is seen in Figure 3.

The time evolution for a field ($\omega = -0.05, h = 0.0022$) is plotted in Figure 4 for several sizes. We can see that the velocity fluctuations after the flip are larger the smaller the system is, showing the size effect mentioned above.

In Figure 5 we show the phase diagram in the space of field parameters (ω, h) resulting from numerical simulations of a system of diameter $L = 72$, concentrated in the region of low frequency and low amplitude of a clockwise ($\omega < 0$) applied field. We observe almost the same behavior as in Figure 2 of reference [19], with a relatively small shift of the threshold values, but, in contrast, "windows" appear here: flip events in regions were no flip was expected, and *vice versa*, non-flip events in regions were flips were expected. We can at present only account, with our calculations in the next sections, for the qualitative mean behavior of our system, including discreteness, finite size and anisotropy only in an approximate way, which does not allow for an explanation of these windows. We consider them as most likely effects of tuning all the parameters of the system $(h, \omega, \lambda, \varepsilon, N)$, because changing slightly any of them, changes considerably the position, extension and even the existence of these windows in the diagram. In addition, for some cases a further factor must be considered: in many simulations, particularly in the longest ones, we have observed destruction of vortices. This was seen to be caused by

- new additional vortices forming in the boundaries due to the magnetic field, diffusing into the lattice. There they can annihilate with the vortices already present, or can escape again towards the boundary, annihilating there with the new corresponding images;
- the original vortex simply annihilates in the boundary with its image, with no additional vortices created during the time of the simulation.

We do not deal with these cases here, because our main concern is studying the flipping time as a rather rapid and clean event with only one vortex. These destruction processes are taken into account only when they occur before the flip of $p \to -p$, giving therefore a finished simulation without flip.

3.3 Trajectories of vortices under influence of an ac magnetic field

One of the aims of this paper is to show that the IP movement of the center of the vortex ("center of mass motion") is to some extent (up to long wavelength spin waves, and modes of the whole lattice produced by the magnetic field) correlated with the OP oscillations of the vortex magnetization, supporting the idea already mentioned in reference [19] that the flipping process needs a finite velocity and the perturbation due to the discrete lattice potential.

The time evolution of both the magnetization of the vortex core and the velocity modulus of the center of the vortex are shown in Figure 1 (above), together with the trajectory of the vortex center (in Fig. 1, below), for some typical strengths of the magnetic field and for a system of diameter $L = 72$, with a single vortex pointing up ($p = 1$) and sitting in the center of the lattice as initial condition. The correlation between both signals can be seen in the zoom-in of a small section in Figure 2. Each maximum and minimum in the magnetization, or maximum in the velocity modulus, in Figure 2 (above), can be identified with a single crossing of a ridge or a saddle of the Peierls-Nabarro potential of the lattice, in Figure 2 (below). The vertices of the grid represent the lattice sites. The section of trajectory shown starts in the center $(0, 0)$ and develops clockwise. The correlation is most evident

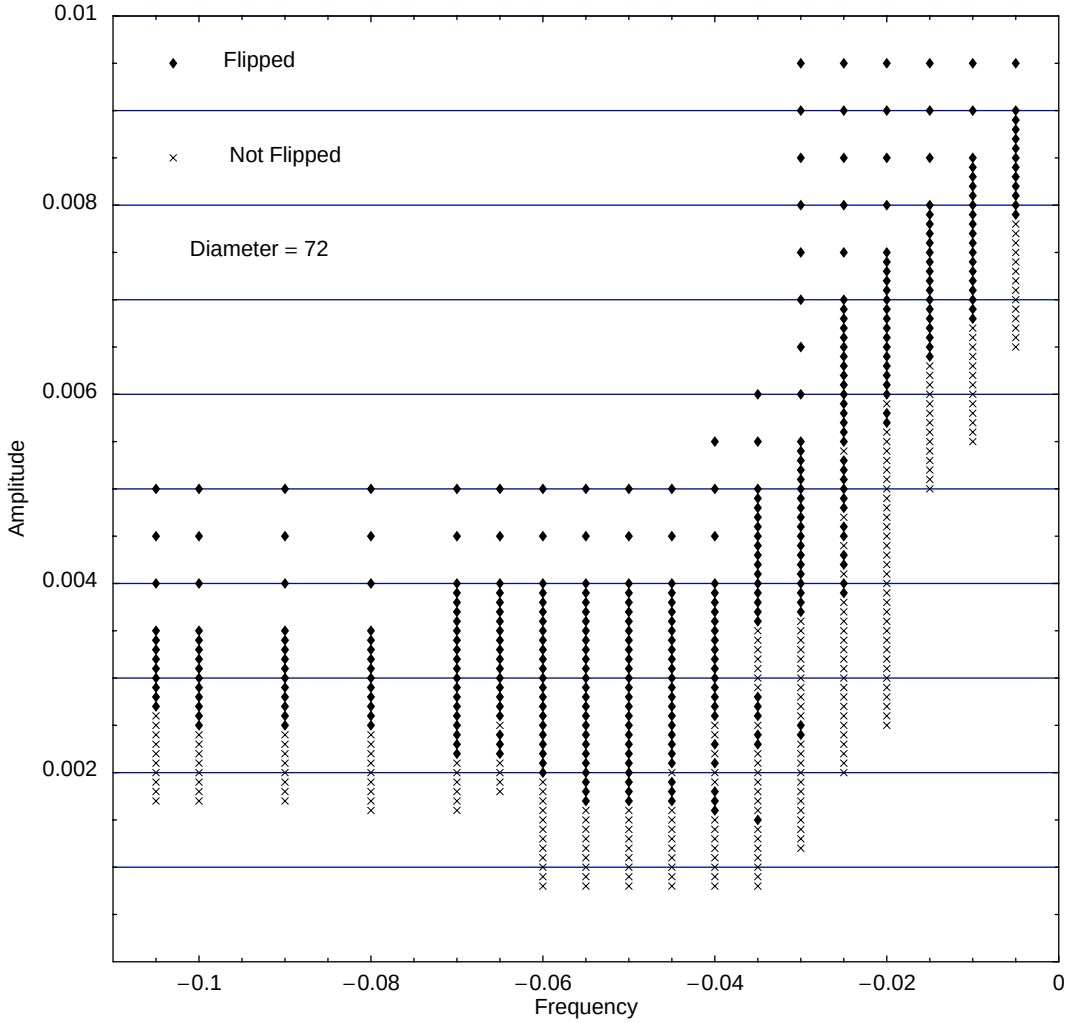

Fig. 5. Phase diagram of flip events in the frequency-amplitude (ω, h) space, for the circular system of diameter $L = 72$, obtained from the numerical integration of the full Landau-Lifshitz equations, with damping $\varepsilon = 0.002$ and anisotropy $\lambda = 0.9$.

before and for some time after the flip. In the immediate time after the flip there are larger fluctuations because the flip itself creates an azimuthally symmetric spin wave which propagates towards the boundary and is reflected there in a non-symmetric way, so that at those times there are many spin waves present. After this transient, the correlation is evident again.

There are several types of trajectories, depending on the frequency ω and amplitude h, that will not be shown here. For $|\omega| \lesssim 0.05$, at not too high amplitudes, we found that the trajectories, after some initial irregularities, spiral out to the boundaries, at the same time smoothing to some regular spiral, as velocities are growing. This shows the change of regime from a "magnetic-field-driven" vortex trajectory, when the vortex is still quite near the center of the lattice, to a regime driven by the interaction with the image vortex, when the vortex is far enough from the center of the lattice. The rate of change in the radius of the trajectories is also affected by the value of the damping.

Instead, for $|\omega| \gtrsim 0.05$ and not too low amplitudes, we found "confining" trajectories, which stay rather long in a strongly irregular pattern, after which they eventually converge to a regular circle, with a relatively small radius. This equilibrium radius is given by a balance between the attraction of the image vortex, and the deflection due to the rotating field, and is, thus, size-dependent. This is actually what happens in the case of the system in Figures 1–2. In the cases when the vortex reaches in the final state a regular circular motion, one can observe the same periodicity in both the velocity and magnetization signals.

This is a simplified summary of trajectories in this complex system. There are other kinds of trajectories which we will discuss in a future paper. For our present purposes it is enough to know that, independently on whether there will be a final "limit cycle" or the vortex at very late times will annihilate at the boundary, in all the cases there is a correlation between out-of-plane oscillations and center of mass movement, like that shown in Figures 1 and 2, which suggests a first hint to understanding the flipping process: the same instability which makes a moving IP vortex develop out-of-plane components for

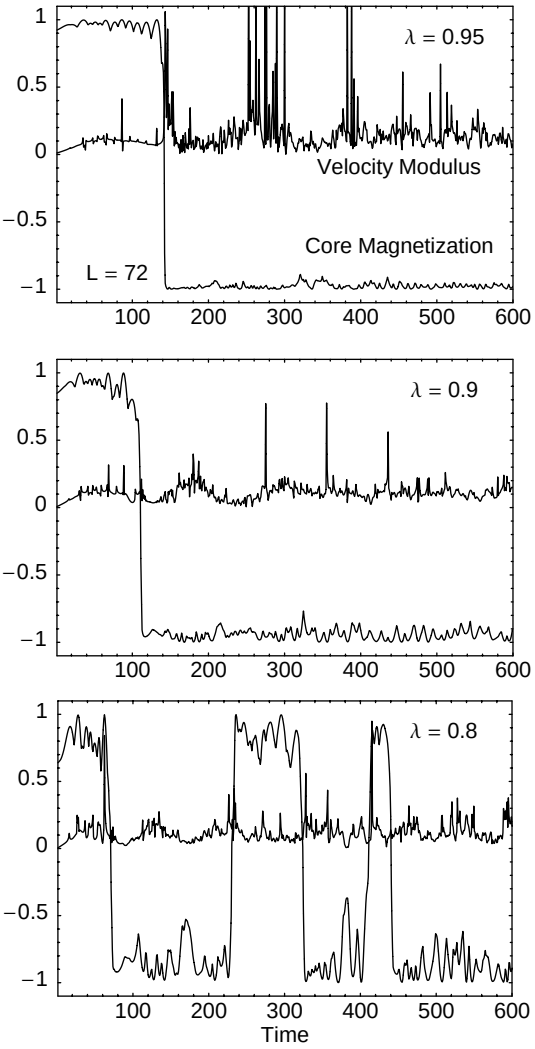

Fig. 6. Time evolution of the vortex core magnetization and velocity modulus, around the flip(s) region, for 3 values of anisotropy $\lambda = 0.8, 0.9, 0.95$ in a clockwise rotating magnetic field for $\omega = -0.025$, $h = 0.0066$, for a system diameter $L = 72$. Note the larger fluctuations and instability of the core magnetization for $\lambda \approx \lambda_c$.

$\lambda > \lambda_c$ [13], should give some contribution to the flipping process of a moving OP vortex. Since all the peaks and minima in the velocity are correlated with the crossing of some ridge or saddle of the Peierls-Nabarro potential, we ascribe them to the discreteness of the lattice. This is also supported in Figure 6, by observing larger fluctuations –even back flip events– for values of λ closer to the critical value $\lambda_c \sim 0.72$. This out-of-plane instability in the presence of anisotropy (discussed in Ref. [15]), will be taken into account in the models of Section 4.

3.4 Simulations with static fields in the rotating frame

An important point of this paper is that we confirmed, in our numerical simulations with a static field containing both an IP component $\boldsymbol{h}_1$ and an OP component $\boldsymbol{h}_2$, as

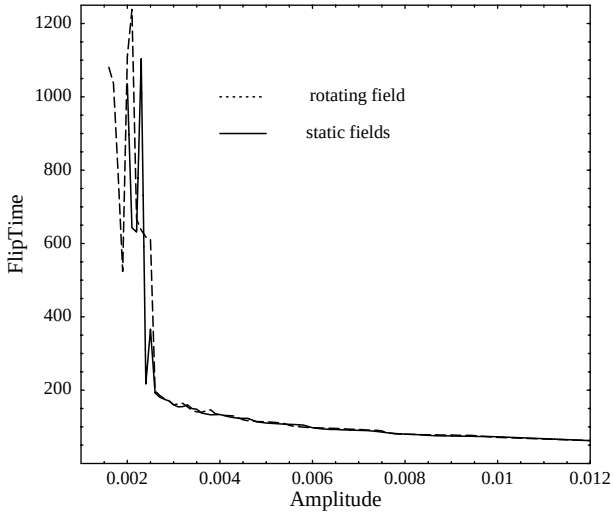

Fig. 7. Comparison of flipping times for 2 different systems: with in-plane rotating field (dashed line) $\omega = -0.05$, *vs.* amplitude h, and (solid line) with a static in-plane and out-of-plane fields $\boldsymbol{h} = (0, h_y, h_z)$, with $h_z = -0.05$, *vs.* h_y. The second system is shown to be equivalent, in the rotating frame, to the first in the static frame. Concerning flip times, we do not need to rotate the spins (by a constant phase for each time) of the second system. System diameter $L = 96$.

mentioned above, the predicted switching behavior. Figure 7 shows a comparison of flipping times for both systems under discussion here. We do not expect the flipping times to be exactly the same, since the equivalence holds strictly in the bulk limit only. The boundaries in both reference frames are clearly different. However, in the cases when the flip occurs relatively close to the center of the lattice, we get better agreement, as the boundary effects are less important. As shown in references [17,18], when a static magnetic field is applied along the hard axis there exist two types of OP vortices in easy-plane ferromagnets: "light" and "heavy" vortices with the gyrovector being parallel and antiparallel to the applied magnetic field, respectively. The energy of the heavy vortex is always higher than the light's one. Therefore the physical reason for switching is obvious: the system transfers from the high energy state (heavy vortex) to the low energy state (light vortex). It is worth mentioning, however, that the presence of an out-of-plane magnetic field is a necessary but not sufficient condition for switching. In the case of a relatively weak OP magnetic field, when the heavy vortex exists as a metastable state of the system, only the presence of an IP component of the static field makes the flipping process possible. This IP component must also be weak in order to keep the vortex confined to the finite system and to have enough time to observe the flip.

4 Discrete core models

As was mentioned in the previous paper [19], the totally symmetric core mode which describes the dynamics of the

vortex polarization does not interact directly with a spatially uniform external magnetic field when the vortex is at the center of the system. Two possibilities were proposed to remove this restriction:

1. In finite systems the vortex moves away from the center due to the interaction with its image, in this way the totally symmetric core mode may be excited.
2. Switching may occur as a result of nonlinear mixing between the totally symmetric mode and nonsymmetric vortex modes, which do interact with the spatially uniform external magnetic field.

Considering in reference [19] relatively small systems, that work assumed that the first mechanism is more important. However, our present numerical simulations showed that the switching process does not depend crucially on the size of the system provided it is large enough (see Fig. 3). Therefore in this paper we will discuss the second mechanism for the switching of vortex polarization.

4.1 Full core model

To gain an insight into how the external magnetic field affects the vortex dynamics we need a reduced form of the Hamiltonian (5) and the interaction (6) which can take into account effectively both IP and OP vortices. We will use a core approach which is a generalization of the approach proposed in reference [15]. We will assume that

i) the in-plane angles $\Phi^0_{\boldsymbol{n}}$ for static in-plane and out-of-plane vortices are given by equation (20), in $X = Y = 0$ without the image contribution;

ii) the deviations of the in-plane angles from their static values $\psi_{\boldsymbol{n}} = \Phi_{\boldsymbol{n}} - \Phi^0_{\boldsymbol{n}}$ and the out-of-plane moments $m_{\boldsymbol{n}}$ rapidly decay with the distance $r_{\boldsymbol{n}} = \sqrt{n_x^2 + n_y^2}$ from the center of the vortex:

$$\psi_{\boldsymbol{n}} = \begin{cases} \psi_1, \text{ for } \boldsymbol{n} = (1/2, 1/2), \\ \psi_2, \text{ for } \boldsymbol{n} = (-1/2, 1/2), \\ \psi_3, \text{ for } \boldsymbol{n} = (-1/2, -1/2), \\ \psi_4, \text{ for } \boldsymbol{n} = (1/2, -1/2), \\ 0, \text{ otherwise} \end{cases} \tag{24}$$

$$m_{\boldsymbol{n}} = \begin{cases} m_1, \text{ for } \boldsymbol{n} = (1/2, 1/2), \\ m_2, \text{ for } \boldsymbol{n} = (-1/2, 1/2), \\ m_3, \text{ for } \boldsymbol{n} = (-1/2, -1/2), \\ m_4, \text{ for } \boldsymbol{n} = (1/2, -1/2), \\ 0, \text{ otherwise.} \end{cases} \tag{25}$$

Thus only the first four spins nearest to the vortex center have non-zero z-components, and appreciable IP deviations from the IP static vortex structure. All other spins lie in the $x-y$ plane, and follow the IP distribution (20). A sketch of this vortex structure can be seen in Figure 8. Under these assumptions the dynamics of the vortex core is described by the following Hamiltonian

$$H_c = -J \sum_{i=1}^{4} \{\lambda\, m_i m_{i+1} + p_i p_{i+1} \sin(\psi_i - \psi_{i+1}) + 2\lambda_c p_i \cos\psi_i\}, \tag{26}$$

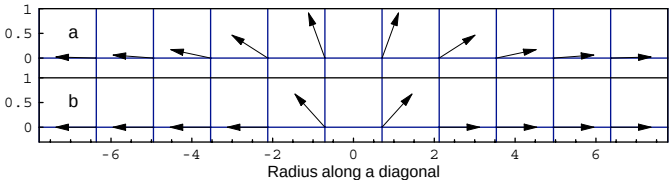

Fig. 8. Section of the out-of-plane structure (z-components) of vortices *vs.* distance along a diagonal of the lattice (separated by $\sqrt{2}$ if $a = 1$), where we chose the initial phase as $\varphi_0 = 0$. In (a): data from the full many spin system with $\lambda = 0.9$, a vortex in the center at $t = 20$ (without magnetic field it does not move). In (b): the vortex used as initial condition in the full core model (28) with $\lambda = 0.95$.

where $p_i = \sqrt{1 - m_i^2}$ and $m_5 \equiv m_1, \psi_5 \equiv \psi_1$. Here $\lambda_c = 2/\sqrt{5} \approx 0.894$, as in the lowest order, "1st-shell" approach for square lattices of reference [15], but in the present approach the four spins are allowed to have different (m_i, ψ_i) values, and the model automatically includes the interaction of this shell with the second (inactive) one. The interaction with the external field (6) takes the form

$$V_c(t) = -h \sum_{i=1}^{4} \sqrt{1 - m_i^2} \cos\left(\psi_i - \omega t - \mathrm{i}\,\frac{\pi}{2}\right) \tag{27}$$

and the equations of motion for the core variables m_i and ψ_i now read

$$\begin{aligned} \frac{\mathrm{d}\psi_i}{\mathrm{d}t} &= \frac{\partial(H_c + V_c)}{\partial m_i} - \frac{\varepsilon}{1 - m_i^2} \frac{\partial H_c}{\partial \psi_i}, \\ \frac{\mathrm{d}m_i}{\mathrm{d}t} &= -\frac{\partial(H_c + V_c)}{\partial \psi_i} - \varepsilon\,(1 - m_i^2)\,\frac{\partial H}{\partial m_i}. \end{aligned} \tag{28}$$

To check the applicability of the core model (26–27), we solved numerically the set of equations (28) and found (Fig. 9) a qualitative agreement with the vortex behavior obtained as a result of the full numerical simulations. The core model gives a rather good global description of the switching process. However, the details of the process are very sensitive to the particular choice of parameters. Changing, for instance, the amplitude or frequency of the field in a fraction smaller than 10^{-4} can give rise to the existence of precursors for the flip, and also back flips. But eventually the switching occurs and the system is locked in the new vortex state.

4.2 Reduced core model

The core model presented in the previous subsection is still rather complicated and to gain deeper insight a further reduction is needed. This can be achieved by considering the behavior of the system near the threshold of IP-OP vortex instability: $(\lambda - \lambda_c)/\lambda_c \ll 1$. It is convenient to introduce instead of m_i and ψ_i the linear combinations which correspond to the four irreducible representations

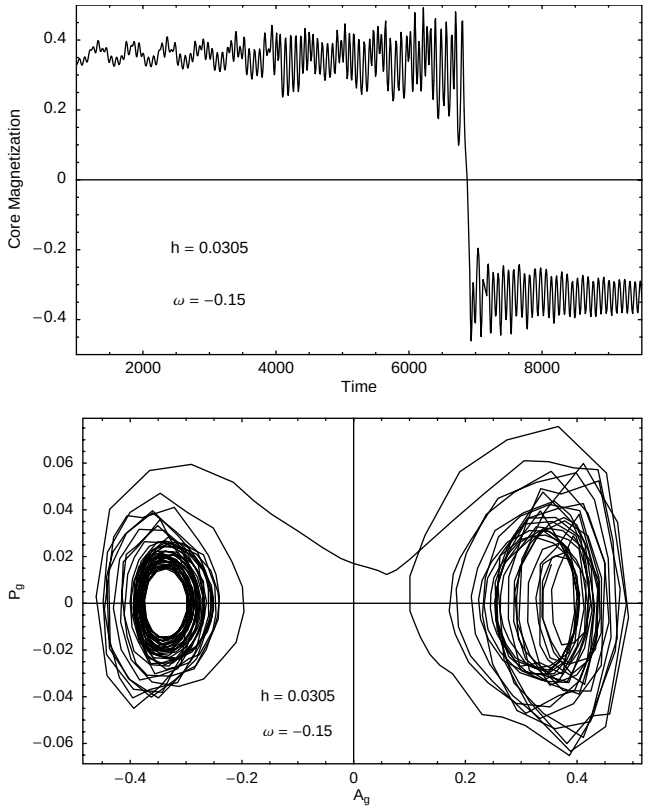

Fig. 9. (above) Time evolution of the core magnetization (average of the m_i) from the numerical solution of the core model of equations (28), with a rotating field of frequency $\omega = -0.15$, and amplitude $h = 0.0305$. Here $J = 1/8$, $\lambda = 0.95$ and $\varepsilon = 0.002$. (below) Projection of the phase trajectory onto the plane of the totally symmetric modes (A_g, P_g) (see Sect. 4.2 for definitions), which here are calculated as averages of the m_i and ψ_i, respectively.

of the site symmetry group of the square (2 inversions, 2 reflexions):

$$\begin{aligned} A_g &= (m_1 + m_2 + m_3 + m_4)/4, \\ P_g &= (\psi_1 + \psi_2 + \psi_3 + \psi_4)/4, \\ B_g &= (m_1 - m_2 + m_3 - m_4)/4, \\ Q_g &= (\psi_1 - \psi_2 + \psi_3 - \psi_4)/4, \\ A_u &= (m_1 + m_2 - m_3 - m_4)/4, \\ P_u &= (\psi_1 + \psi_2 - \psi_3 - \psi_4)/4, \\ B_u &= (m_1 - m_2 - m_3 + m_4)/4, \\ Q_u &= (\psi_1 - \psi_2 - \psi_3 + \psi_4)/4. \end{aligned} \tag{29}$$

For instance, the A_g, P_g-mode is totally symmetric under reflections ($1 \leftrightarrow 2$ and $3 \leftrightarrow 4$, or $1 \leftrightarrow 4$ and $2 \leftrightarrow 3$) and inversions ($1 \leftrightarrow 3$ or $2 \leftrightarrow 4$), the B_g, Q_g-mode is inversion-symmetric and reflection-antisymmetric, and so on. It was shown in references [15,31] that the totally symmetric mode, when all core spins move in phase, is responsible for the instability of IP vortices in easy-plane ferromagnets with weak anisotropy. Therefore, to take into account the soft character of this mode, we will consider the totally symmetric A_g, P_g-mode as a nonlinear one, while all other modes will be considered in the harmonic approximation. By inserting equation (29) into equation (26) and expanding the corresponding Hamiltonian we get

$$H_c = -16J\lambda_c + H_s + H_{ns} + H_u, \tag{30}$$

where

$$H_s = 8J\left\{\frac{1}{2}(\lambda_c - \lambda)A_g^2 + \frac{1}{8}\lambda_c A_g^4 + \frac{1}{2}\lambda_c P_g^2\right\} \tag{31}$$

is the Hamiltonian of the totally symmetric mode,

$$H_{ns} = 8J\left\{\frac{1}{2}\lambda_c Q_g^2 + \frac{1}{2}(\lambda + \lambda_c)B_g^2\right\} \tag{32}$$

is the Hamiltonian of the non-symmetric g-mode, and

$$\begin{aligned} H_u = 8J\Big\{&\frac{1}{2}\lambda_c\left(A_u^2 + B_u^2 + P_u^2 + Q_u^2\right) \\ &+ A_g\left(A_u Q_u - P_u B_u\right)\Big\} \end{aligned} \tag{33}$$

is the part of the core Hamiltonian which describes the antisymmetric u-modes. In the same approximation the interaction Hamiltonian (27) is expressed as follows

$$\begin{aligned} V_c(t) = &-2h\left[Q_u - P_u + A_g(A_u + B_u) + P_g(P_u + Q_u)\right] \\ &\times \sin(\omega t) - 2h\left[Q_u + P_u + A_g(A_u - B_u)\right. \\ &\left.+ P_g(P_u - Q_u)\right]\cos(\omega t). \end{aligned} \tag{34}$$

In terms of the new variables (29) the equations of motion (28) read

$$\begin{aligned} \frac{\mathrm{d}A_\nu}{\mathrm{d}t} &= -\frac{\partial}{\partial P_\nu}\left[H + V_c(t)\right] - \varepsilon\frac{\partial H}{\partial A_\nu}, \\ \frac{\mathrm{d}P_\nu}{\mathrm{d}t} &= \frac{\partial}{\partial A_\nu}\left[H + V_c(t)\right] - \varepsilon\frac{\partial H}{\partial P_\nu}, \\ \frac{\mathrm{d}B_\nu}{\mathrm{d}t} &= -\frac{\partial}{\partial Q_\nu}\left[H + V_c(t)\right] - \varepsilon\frac{\partial H}{\partial B_\nu}, \\ \frac{\mathrm{d}Q_\nu}{\mathrm{d}t} &= \frac{\partial}{\partial B_\nu}\left[H + V_c(t)\right] - \varepsilon\frac{\partial H}{\partial Q_\nu}, \end{aligned} \tag{35}$$

where $\nu = u, g$ and it was taken into account that for $(\lambda - \lambda_c)/\lambda_c \ll 1$ the out-of-plane components m_i are small and therefore in equations (35) small terms εA_ν^2 and B_ν^2 were omitted.

Let us first consider the eigenmodes of the Hamiltonian (30). For the no-driving case ($h = 0$) the equations of motion for the modes (29) read

$$\begin{aligned} \dot{A}_g &= -8J\,\lambda_c P_g, \\ \dot{P}_g &= 8J\left\{(\lambda_c - \lambda)A_g + \frac{1}{2}\lambda_c A_g^3 + A_u Q_u - P_u B_u\right\}, \\ \dot{B}_g &= -8J\,\lambda_c Q_g, \\ \dot{Q}_g &= 8J\,(\lambda + \lambda_c)B_g, \end{aligned} \tag{36}$$

$$\begin{aligned} \dot{A}_u &= 8J\,(-\lambda_c P_u + A_g B_u), \\ \dot{P}_u &= 8J\,(\lambda_c A_u + A_g Q_u), \\ \dot{B}_u &= 8J\,(-\lambda_c Q_u - A_g A_u), \\ \dot{Q}_u &= 8J\,(\lambda_c B_u - A_g P_u), \end{aligned} \tag{37}$$

where $\dot{x} \equiv \frac{\mathrm{d}x}{\mathrm{d}t}$. When $\lambda < \lambda_c$ (IP vortex is stable) the equilibrium state of the Hamiltonian (31) is achieved for $A_g = 0$, $P_g = 0$. Near this state the second term on the r.h.s. of the second of equations (36), as well as the last terms on the r.h.s of equations (37), are small and may be omitted in the harmonic approximation. Under these conditions the totally symmetric A_g, P_g-mode is characterized by the eigenfrequency $\omega_{in} = 8J\sqrt{\lambda_c(\lambda_c - \lambda)}$. The B_g, Q_g-mode is decoupled and oscillates with the eigenfrequency $8J\sqrt{\lambda_c(\lambda_c + \lambda)}$. The A_u, P_u- and B_u, Q_u-modes also result in decoupled eigenmodes of the system, both with the same frequency $8J\lambda_c$. Note that the totally symmetric A_g, P_g-mode is the only one which requires $\lambda < \lambda_c$.

When $\lambda > \lambda_c$ (OP vortex is stable) the Hamiltonian (31) possesses two minima $P_g = 0$, $A_g = \pm\sqrt{2(\lambda - \lambda_c)/\lambda} := \pm m_0$ (m_0 has the meaning of core magnetization). For the OP vortex the frequency of the totally symmetric eigenmode is given by $\omega_{out} = 8J\sqrt{2\lambda_c(\lambda - \lambda_c)}$. It follows from equations (37) that in this case the antisymmetric eigenmodes are

$$\chi_+ = \frac{1}{2}\left(A_u + Q_u - \mathrm{i}(B_u - P_u)\right),$$
$$\chi_- = \frac{1}{2}\left(A_u - Q_u + \mathrm{i}(B_u + P_u)\right) \qquad (38)$$

and χ_+^*, χ_-^*, with the corresponding eigenfrequencies

$$\omega_\pm = 8J(\lambda_c \pm m_0). \qquad (39)$$

In the driving case when $h \neq 0$, inserting equations (38) into equations (33, 34) we get

$$H_u = 8J\left\{(\lambda_c + A_g)|\chi_+|^2 + (\lambda_c - A_g)|\chi_-|^2\right\}, \quad (40)$$

$$V_c(t) = h\,(\mathrm{i} - 1)[(-1 + A_g - \mathrm{i}P_g)\chi_- + (1 + A_g + \mathrm{i}P_g)\chi_+^*]\,\mathrm{e}^{\mathrm{i}\omega t} + \mathrm{c.c.} \qquad (41)$$

Note that χ_μ and χ_μ^* ($\mu = \pm$) are now canonically conjugated variables with the equations of motion in the form

$$\dot{\chi}_\mu = \mathrm{i}\frac{\partial\,(H + V_c(t))}{\partial \chi_\mu^*} - \varepsilon\frac{\partial H}{\partial \chi_\mu^*}, \qquad (42)$$

where the Hamiltonian H is given by $H = H_s + H_u$.

As can be seen from equations (41, 29) the interaction $V_c(t)$ vanishes in the case of the totally symmetric A_g, P_g-mode. Therefore, *switching processes under the action of the spatially uniform magnetic field can occur only as a result of nonlinear mixing between the totally symmetric mode and antisymmetric core modes, where the latter ones do interact with the spatially uniform alternating external field.*

It is worth noting that the antisymmetric $\chi_\pm$ modes may be identified with the two lowest modes $T_\pm$ of reference [33] that produce the cycloidal orbital motion of the vortex center [33,34]. The equations of motion for the $\chi_\pm$ modes

$$\dot{\chi}_+ = \mathrm{i}8J(\lambda_c + A_g)\chi_+ - 8J\varepsilon\chi_+ + h\,(1 - \mathrm{i})(1 + A_g + \mathrm{i}P_g)\,\mathrm{e}^{\mathrm{i}\omega t}, \qquad (43)$$

$$\dot{\chi}_- = \mathrm{i}8J(\lambda_c - A_g)\chi_- - 8J\varepsilon\chi_- + h\,(\mathrm{i} + 1)(1 - A_g - \mathrm{i}P_g)\,\mathrm{e}^{\mathrm{i}\omega t}, \qquad (44)$$

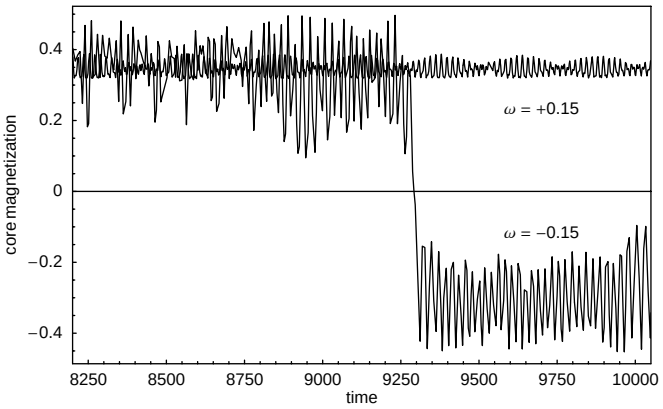

Fig. 10. Time evolution of the core magnetization A_g, for amplitude $h = 0.05$ and two opposite frequencies $\omega = \pm 0.05$, from the numerical solution of the reduced core model of equations (30–35). Here $J = 1/8$, $\lambda = 0.95$ and $\varepsilon = 10^{-4}$.

can be thought of as a microscopic version of the Thiele equations (see Appendix B) where the gyrovector modulus $G \sim A_g$ is a time dependent quantity which is governed by the equations

$$\dot{A}_g = -8J(\lambda_c P_g + \varepsilon A_g) + h(\mathrm{i} + 1)(\chi_-^* - \chi_+)\,\mathrm{e}^{\mathrm{i}\omega t} + h(1 - \mathrm{i})(\chi_- - \chi_+^*)\,\mathrm{e}^{-\mathrm{i}\omega t}, \qquad (45)$$

$$\dot{P}_g = 8J\left[(\lambda_c - \lambda)A_g + \frac{A_g^3}{2} + |\chi_+|^2 - |\chi_-|^2 - \varepsilon P_g\right] + h(\mathrm{i} - 1)(\chi_-^* + \chi_+)\,\mathrm{e}^{\mathrm{i}\omega t} - h(1 + \mathrm{i})(\chi_- + \chi_+^*)\,\mathrm{e}^{-\mathrm{i}\omega t}. \qquad (46)$$

Thus the modes χ_μ (the orbital motion) are excited by the external magnetic field (4) and they in turn act as drivers giving impetus to the switching dynamics of the vortex. In Figure 10 we present the time evolution of the core magnetization A_g for two opposite frequencies of the field, based on numerical integration of the reduced core model (30–35). The distinction between the action of clockwise- and counterclockwise-rotating magnetic fields is clearly seen. It should also be mentioned that in the framework of the reduced model the unidirectional character of flipping events is not so well pronounced. As a rule, a significant part of time the system is in a state when back and forth flips take place. This is, however, in agreement with our full simulations of the LL equations (3) which show the same behavior in the near-critical case $\lambda \approx \lambda_c$ for which the reduced model was derived, see Figure 6.

5 Conclusions

In this work we have investigated the phenomenon of switching of the out-of-plane vortex magnetization, driven by a rotating magnetic field. Our results may be summarized as follows:

- Flipping times do not depend essentially on the size of the system, provided that the lattice is large enough (diameter $L \gtrsim 72$). In other words, the switching of the

vortex polarization is not much affected by the presence of boundaries.

• A clear correlation exists between the core magnetization dynamics (the oscillations of the core spins in the perpendicular-to-plane direction) and the velocity of the vortex center in the plane of the lattice.

• A phase diagram of flipping events from extensive numerical simulations with an OP vortex in a rotating magnetic field was presented. We found that in the (ω, h) phase space there is no well-defined curve which separates the region where the flips do not occur from the region where they do. For a given frequency ω and increasing amplitude h we find intervals ("windows") of intermittent flip- and nonflip- events.

• The switching process is unidirectional only if the anisotropy parameter λ is not too close to the critical value λ_c. The closer λ is to λ_c, the more unstable the system is against flips of the vortex polarization in a weak field, and the larger fluctuations of the vortex core magnetization are observed.

• Switching of the vortex polarization can be achieved also by applying a static magnetic field with both in-plane and out-of-plane components.

• The switching dynamics may be described in terms of a generalized Thiele equation which takes into account a coupling between the vortex polarization dynamics and the motion of the vortex center.

It is clear that the phenomenon of switching we describe will not be essentially affected by the inclusion of magnetostatic interaction. The shape of the vortex core and the far field will be only slightly modified by this interaction. The flipping process has to do essentially with the externally applied magnetic field. The experimental works on nanodisks mentioned in the Introduction already reported [1,2,4] the observation of vortices in either of two polarization states, and the switching between them was forced by means of static fields perpendicular to the disks. Our theoretical work qualitatively suggests that it would be interesting as well to apply weak rotating fields, like those used here, to control both the mean position of a vortex in larger magnetic dots (where the vortex center could show dynamics) and at the same time the sign of the out-of-plane core magnetization.

Juan P. Zagorodny acknowledges rich discussions with Prof. F. Waldner, Zürich, and kind help of Dr. T. Kamppeter, Paris. Work supported by Deutsche Forschungsgemeinschaft, at the University of Bayreuth. Yuri Gaididei thanks for the hospitality of the University of Bayreuth, and also acknowledges the support provided by the DLR Project No. UKR-002-99. Alan Bishop is a Humboldt awardee at the University of Bayreuth.

Appendix A: Remarks on the form of damping terms

The Gilbert form of the LL equations with damping [21], in normalized variables, reads

$$\frac{\mathrm{d}\boldsymbol{S_n}}{\mathrm{d}t} = \boldsymbol{S_n} \times \boldsymbol{B_n} - \varepsilon\, \boldsymbol{S_n} \times \frac{\mathrm{d}\boldsymbol{S_n}}{\mathrm{d}t}, \tag{A.1}$$

where

$$\begin{aligned} \boldsymbol{B_n} &= -\frac{\delta\,[H + V(t)]}{\delta \boldsymbol{S_n}} \equiv \boldsymbol{F_n} + \boldsymbol{h_n}(t) \\ &= J \sum_{\boldsymbol{a}} \left(S^x_{\boldsymbol{n+a}},\ S^y_{\boldsymbol{n+a}},\ \lambda\, S^z_{\boldsymbol{n+a}}\right) + \boldsymbol{h_n}(t) \end{aligned} \tag{A.2}$$

is the effective field each spin feels because of the action of its neighbors and the external magnetic field. One can transform these equations replacing the value of $\frac{\mathrm{d}\boldsymbol{S_n}}{\mathrm{d}t}$ on the r.h.s. and bringing it to the l.h.s. By taking into account the constraint $|\boldsymbol{S_n}| = S$, one gets

$$\left(1 + \varepsilon^2 S^2\right) \frac{d\boldsymbol{S_n}}{dt} = \boldsymbol{S_n} \times \boldsymbol{B_n} - \varepsilon\, \boldsymbol{S_n} \times \boldsymbol{S_n} \times \boldsymbol{B_n}, \tag{A.3}$$

which, after a proper rescaling of the time variable, is the (normalized) Landau form [21]. As Iida pointed out [21], these two equations are, though, as just seen, mathematically equivalent, not physically equivalent, and arguments are given to show that (A.3) contains anisotropic damping while in (A.1) the damping is isotropic. However, numerical integration can be done only once we have solved for $\mathrm{d}\boldsymbol{S_n}/\mathrm{d}t$ as in (A.3). This last equation is not mathematically equivalent to (3), *i.e.*,

$$\frac{\mathrm{d}\boldsymbol{S_n}}{\mathrm{d}t} = \boldsymbol{S_n} \times \boldsymbol{B_n} - \varepsilon\, \boldsymbol{S_n} \times \boldsymbol{S_n} \times \boldsymbol{F_n}, \tag{A.4}$$

mainly because the magnetic field is not present in the second term of the latter. Nevertheless, we should expect no great differences, since as stated above we are interested in small amplitudes h ($\sim 10^{-3}$) and damping ε ($\sim 10^{-3}$). We can neglect the $\mathcal{O}(\varepsilon^2)$ in the prefactor of equation (A.3) (which is in turn equivalent to a normalization of the time variable [21], together with a corresponding change in the frequency) and also the contribution of $\mathcal{O}(\varepsilon h)$ in the second term on the r.h.s. of (A.3), giving (3) or (A.4). From the relaxation viewpoint, taking the dynamics (A.3) one easily derives

$$\frac{\mathrm{d}H}{\mathrm{d}t} = -\varepsilon \sum_n \Big[\boldsymbol{S}_n \times \boldsymbol{B}_n\Big]^2 - \sum_n \boldsymbol{S}_n \cdot \frac{\mathrm{d}\boldsymbol{h}_n(t)}{\mathrm{d}t} \tag{A.5}$$

while taking the dynamics (A.4) one has

$$\begin{aligned} \frac{\mathrm{d}H}{\mathrm{d}t} = &-\ \varepsilon \sum_n \Big[\boldsymbol{S}_n \times \boldsymbol{F}_n\Big]^2 - \sum_n \boldsymbol{S}_n \cdot \frac{\mathrm{d}\boldsymbol{h}_n(t)}{\mathrm{d}t} \\ &-\ \varepsilon \sum_n \big(\boldsymbol{S}_n \times \boldsymbol{F}_n\big) \cdot \big(\boldsymbol{S}_n \times \boldsymbol{h}_n(t)\big). \end{aligned} \tag{A.6}$$

In our computer simulations, with $\varepsilon = 0.002$, it turned out that the first terms, $\mathcal{O}(\varepsilon)$, and second terms, $\mathcal{O}(\omega h)$,

of both equations are the dominant ones, and so the difference, *i.e.* two terms of $\mathcal{O}(\varepsilon h^2)$ and $\mathcal{O}(\varepsilon h)$, is negligible for all the values of h and ω we used. In all the cases we found quickly relaxing oscillations for the signal of energy *vs.* time. We also checked the accuracy of our approximation in our computer simulations, by comparing the flipping times and vortex trajectories given by equations (A.3, A.4) [or (3)], and it turned out that the differences arising from their two different damping terms are negligible, at the value of damping we have used. In particular, the switching of polarization remains unchanged. From the numerical viewpoint, the effort in simulating the two equations is the same. Since the physics is not essentially changed by using one or the other equation, we have chosen to use the form (3) in our analysis, because it allows the argument leading to the presence of effective static fields, in equations (21–23) of Section 2.2. On the other hand, it should be stressed here that the theory of magnetic damping stays at the present time in a phenomenological stage. New developments like those of Baryakhtar and coworkers are under experimental test [22].

Appendix B: Connection with a generalized Thiele equation

In the continuum limit the dynamics of the vortex position $\boldsymbol{R}(t) = (X(t), Y(t), 0)$ is described by some generalized Thiele equation up to some given order in time derivatives of $\boldsymbol{R}(t)$ [25]. For our purposes, here it is enough to use the second order equation with mass [33],

$$M_v\,\ddot{\boldsymbol{R}} - \boldsymbol{G}\times\dot{\boldsymbol{R}} = -\frac{\partial}{\partial \boldsymbol{R}}\,U(\boldsymbol{R}), \tag{B.1}$$

where $U(\boldsymbol{R})$ is a potential energy (due to possible external magnetic fields, interactions with other vortices and the discreteness of the lattice [26,27,33]), M_v has the meaning of the effective mass of the vortex and $\boldsymbol{G} = 2\pi pq\hat{z} = G\hat{z}$ is the gyrovector for the vortex with polarization $p = \pm 1$ and circulation charge q. Equation (B.1) can be obtained from the Lagrangian

$$L_{Th} = \frac{M_v}{2}\left(\dot{X}^2 + \dot{Y}^2\right) + \frac{G}{2}\left(Y\dot{X} - X\dot{Y}\right) - U(\boldsymbol{R}). \tag{B.2}$$

The Hamiltonian which corresponds to the Thiele equation (B.1) may be obtained by using a Legendre transformation [37], namely

$$H_{Th} = \dot{X}\,P_X + \dot{Y}\,P_Y - L_{Th}, \tag{B.3}$$

where

$$\begin{aligned} P_X &= \frac{\partial L_{Th}}{\partial \dot{X}} = M_v\,\dot{X} + \frac{G}{2}\,Y \\ P_Y &= \frac{\partial L_{Th}}{\partial \dot{Y}} = M_v\,\dot{Y} - \frac{G}{2}\,X \end{aligned} \tag{B.4}$$

are the components of the canonically conjugated momentum $\boldsymbol{P}$. Inserting equations (B.4) into equation (B.3) we obtain a Hamiltonian in the form

$$\begin{aligned} H_{Th} = {} & \frac{1}{2M_v}\left(P_X^2 + P_Y^2\right) + \frac{G}{2M_v}\left(P_Y\,X - P_X\,Y\right) \\ & + \frac{G^2}{4M_v}\left(X^2 + Y^2\right) + U(\boldsymbol{R}). \end{aligned} \tag{B.5}$$

In the vicinity of the minimum of the Peierls-Nabarro potential the potential function $U(\boldsymbol{R})$ may be approximately presented in the form

$$U(\boldsymbol{R}) = \frac{1}{2}\,\kappa\,|\boldsymbol{R}|^2, \tag{B.6}$$

where the coefficient κ characterizes the steepness of the Peierls-Nabarro potential. Comparing the Hamiltonian of equations (B.5, B.6) with the Hamiltonian (33) which describes the dynamics of the antisymmetric core modes, we see that they have the same structure if we put

$$\frac{1}{M_v} = \mathcal{J}\lambda_c, \quad \frac{G}{2M_v} = \mathcal{J}A_g, \quad \frac{G^2}{4M_v} + \kappa = \mathcal{J}\lambda_c, \tag{B.7}$$

where $\mathcal{J}$ is a common scaling parameter. The same procedure can be given for 3rd order Thiele equations, and a link can be found between the corresponding Lagrangian and a reduced model in which one must keep higher orders in the treatment of the antisymmetric modes.

References

1. T. Shinjo, T. Okuno, R. Hassdorf, K. Shigeto, T. Ono, Science **289**, 930 (2000)
2. J. Raabe, R. Pulwey, R. Sattler, T. Schweinböck, J. Zweck, D. Weiss, J. Appl. Phys. **88**, 4437 (2000)
3. A. Fernandez, C.J. Cerjian, J. Appl. Phys. **87**, 1395 (2000)
4. M. Schneider, H. Hoffmann, J. Zweck, Appl. Phys. Lett. **77**, 2909 (2000)
5. R.P. Cowburn, D.K. Koltsov, A.O. Adeyeye, M.E. Welland, D.M. Tricker, Phys. Rev. Lett. **83**, 1042 (1999)
6. A.R. Völkel, A.R. Bishop, F.G. Mertens, G.M. Wysin, J. Phys. B **4**, 9411 (1992); K. Hirakawa, H. Yoshizawa, K. Ubukoshi, J. Phys. Soc. Jpn **51**, 2151 (1982)
7. A. Hubert, R. Schäfer, *Magnetic Domains* (Springer-Verlag, Berlin, 1998)
8. *Magnetic Properties of Layered Transition Metal Compounds*, edited by J. de Jongh Kluwer (Academic Publishers, Dortdrecht, 1990)
9. F.G. Mertens, A.R. Bishop, in *Nonlinear Science at the dawn of the 21st century*, edited by P.L. Christiansen, M.P. Soerensen, A.C. Scott, Lecture Notes in Physics (Springer, Berlin, 2000)
10. V.L. Berezinskii, Sov. Phys. JETP **32**, 493 (1970); **34**, 610 (1972). J.M. Kosterlitz, D.J. Thouless, J. Phys. C **6**, 1181 (1973). J.M. Kosterlitz, J. Phys. C **7**, 1046 (1974)
11. A.A. Belavin, A.M. Polyakov, JETP Lett. **22**, 245 (1975). S. Trimper, Phys. Lett. **70A**, 114 (1979)
12. S. Hikami, T. Tsuneto, Prog. Theor. Phys. **63**, 387 (1980). A.V. Nikiforov, E.B. Sonin, Sov. Phys. JETP **58**, 373 (1983)

13. M.E. Gouvêa, G.M. Wysin, A.R. Bishop, F.G. Mertens, Phys. Rev. B **39**, 11840 (1989)
14. F.G. Mertens, A.R. Bishop, G.M. Wysin, C. Kawabata, Phys. Rev. Lett. **59**, 117 (1987); Phys. Rev. B **39**, 591 (1989)
15. G.M. Wysin, Phys. Rev. B **49**, 8780 (1994)
16. M.E. Gouvêa, G.M. Wysin, A.S. Pires, Phys. Rev. B **55**, 14 144 (1997) M.E. Gouvêa, F.G. Mertens, A.R. Bishop, G.M. Wysin, J. Phys. Cond. Matt. **2**, 1853 (1990)
17. B.A. Ivanov, D. Sheka, Low Temp. Phys. **21**, 881 (1995)
18. B.A. Ivanov, G.M. Wysin, Phys. Rev. B **65**, 134434 (2002)
19. Yu. Gaididei, T. Kampetter, F. Mertens, A.R. Bishop, Phys. Rev. B **61**, 9449 (2000)
20. V.L. Pokrovskiĭ, G.V. Uĭmin, JETP Lett. **41**, 128 (1985)
21. S. Iida, J. Phys. Chem. Solids **24**, 625 (1963). L.D. Landau, E. Lifshitz, Phys. Z. Sowjetunion **8**, 153 (1935)
22. V.G. Baryakhtar, B.A. Ivanov, A.L. Sukstanskii, E.Y. Melikhov, Phys. Rev. B **56**, 619 (1997)
23. B.A. Ivanov, A.K. Kolezhuk, Low Temp. Phys. **21**, 275 (1995). A.M. Kosevich, B.A. Ivanov, A.S. Kovalev, Phys. Rep. **194**, 117 (1990)
24. S. Komineas, N. Papanicolaou, Physica D, **99**, 81 (1996). N. Papanicolaou, T.N. Tomaras, Nuc. Phys. B **360**, 425 (1991)
25. F.G. Mertens, H.J. Schnitzer, A.R. Bishop, Phys. Rev. B **56**, 2510 (1997)
26. A.A. Thiele, Phys. Rev. Lett. **30**, 230 (1973)
27. D.L. Huber, Phys. Rev. B **26**, 3758 (1982)
28. G.M. Wysin, F.G. Mertens, A.R. Völkel, A.R. Bishop, in *Nonlinear Coherent Structures in Physics and Biology*, edited by K.H. Spatschek, F.G. Mertens (Plenum, New York, 1994)
29. A.M. Kosevich, V.P. Voronov, I.V. Manzhos, Sov. Phys. JETP **57**, 86 (1983)
30. Yu. Gaididei, T. Kampetter, F. Mertens, A.R. Bishop, Phys. Rev. B **59**, 7010 (1999)
31. G.M. Wysin, A.R. Völkel, Phys. Rev. B **52**, 7412 (1995)
32. B.A. Ivanov, H.J. Schnitzer, F.G. Mertens, G.M. Wysin, Phys. Rev. B **58**, 8464 (1998)
33. G.M. Wysin, Phys. Rev. B **54**, 15156 (1996)
34. A.S. Kovalev, F.G. Mertens, H.J. Schnitzer, submitted to Eur. Phys. J. B (2003)
35. A.R. Völkel, F.G. Mertens, A.R. Bishop, G.M. Wysin, Phys. Rev. B **43**, 5992 (1991)
36. *Spin Dynamics in Confined Magnetic Structures I*, edited by B. Hillebrands, K. Ounadjela, Topics in Applied Physics **83** (2002)
37. L.D. Landau, E.M. Lifshitz, *Course of Theoretical Physics I: Mechanics* (Pergamon Press, 1960)